Understanding the selectivity of inhibitors toward PI4KIIIα and PI4KIIIβ based molecular modeling

Tian, Shuaizhen; Zeng, Jinzhe; Liu, Xiao; et.al.

Tian, S., Zeng, J., Liu, X., Chen, J., Zhang, J. Z. H., & Zhu, T. (2019). Understanding the selectivity of inhibitors toward PI4KIIIα and PI4KIIIβ based molecular modeling. In Physical chemistry chemical physics (Vol. 21, Issue 39, pp. 22103–22112). Royal Society of Chemistry. https://doi.org/10.7282/00000189
Document Version: Accepted Manuscript (AM)

View Article Online
DOI: 10.1039/C9CP03598B

Understanding the selectivity of inhibitors toward PI4KIIIα and PI4KIIIβ based molecular modeling

Shuaizhen Tian[a], Jinzhe Zeng[a], XiaoLiu[b,*], Jianzhong Chen[c], John ZH Zhang[a,d] and Tong Zhu[a,d,*]

[a]Shanghai Engineering Research Center of Molecular Therapeutics & New Drug Development, School of Chemistry and Molecular Engineering, East China Normal University, Shanghai, 200062, China
[b]School of Mathematics, Physics and Statistics, Shanghai University of Engineering Science, Shanghai 201620, China
[c]School of Science, Shandong Jiaotong University, Jinan 250357, China
[c]NYU-ECNU Center for Computational Chemistry at NYU Shanghai, Shanghai, 200062, China
* Corresponding authors: liuxiaode2013@163.com (X.L.), tzhu@lps.ecun.edu.cn (T.Z.).

Abstract: Type III phosphatidylinositol 4 kinases (PI4KIIIs) are essential enzymes that relating to the replication of multiple RNA viruses. Understanding the interaction mechanism of molecular compounds with the alpha and beta isoforms of PI4KIII (PI4KIIIα and PI4KIIIβ) is of significance in the development of inhibitors which can bind to these two enzymes selectively. In this work, molecular dynamics (MD) simulations and binding free energy calculations were combined to investigate the binding modes of seven selected compounds to PI4KIIIα and PI4KIIIβ. Analyses based on MD trajectories provide detailed interaction mechanisms of these compounds with PI4KIIIα and PI4KIIIβ at the atomic level, and indicate that the selectivity of these compounds is mainly due to the structural difference of the binding pockets. It is expected that detailed binding information found in this study can provide useful help for the structure-based design of selective inhibitors toward PI4KIIIα and PI4KIIIβ.

View Article Online
DOI: 10.1039/C9CP03598B

Introduction

It is well known that phosphatidylinositol 4-kinases (PI4Ks) play an essential role in the synthesis of phosphatidylinositol 4-phosphate (PI4P). PI4P not only act as the primary lipid determinant of the Golgi and trans-Golgi network (TGN) [1] but also assist the plasma membrane to define the acidic character [2]. PI4P is also an essential precursor for other multiply phosphorylated signaling lipids, such as phosphatidylinositol 3,4,5-trisphosphate (PIP3) and phosphatidylinositol 4,5-trisphosphate (PIP2) [3]. Additionally, PI4P was considered as an essential molecule in signaling and cellular trafficking, especially for in the Golgi and TGN [4-6]. By now, four PI4Ks in humans have been identified, including two type II enzymes (PI4KIIα and PI4KIIβ) and two type III enzymes (PI4KIIIα and PI4KIIIβ, Figure 1).

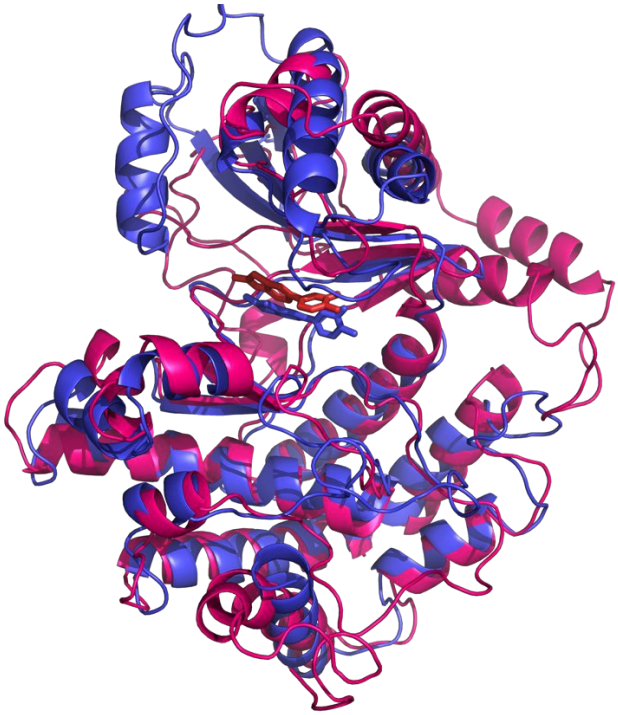

Figure 1. Superposition of the catalytic domain of PI4KIIIα (pink, homology modeling structure) and PI4KIIIβ (blue, PDB ID: 4D0L)

Many studies have shown that PI4KIIIα is a key host factor for the replication of hepatitis C virus (HCV) [7-11], a virus leading cause of chronic liver disease. An investigation suggests that ~80 million people around the world were infected by HCV [12]. In fact, HCV can interact directly with PI4KIIIα by its NS5A protein and stimulate the activity of PI4KIIIα [13]. Furthermore, silencing the PI4KIIIα gene was proved to induce aberrant web morphology and inhibited the HCV's replication [14]. Therefore, designing rational compound which targeting PI4KIIIα is a valuable approach for the treatment of HCV. PI4KIIIβ is mainly localized in the Golgi [15, 16] and is essential for the replication of some RNA virus as it produces a PI4P lipid microenvironment [17]. For example, a number of RNA viruses, including poliovirus, coxsackieviruses, enterovirus, rhinovirus, and Aichi virus [8, 17-21], highly depend on the mediating effect of PI4KIIIβ. Thus, PI4KIIIβ has also been regarded as a potential pharmacological target due to its important role in the multiplication of many viruses.

View Article Online
DOI: 10.1039/C9CP03598B

In the past few years, a series of compounds that inhibit type III PI4Ks have been reported. Some compounds have selectivity toward PI4KIIIα [22-25], while some compounds are more sensitive to PI4KIIIβ [26-35]. Certainly, there are still some compounds do not have obvious selectivity toward PI4KIIIα and PI4KIIIβ [36-39]. So far, it is still not fully understood how those compounds target type III PI4Ks selectively. Thus, probing the interaction mechanism of compounds toward type III PI4Ks is of significance for the design of potent inhibitors in the future. In this work, seven compounds (Figure 2) which have different selectivity toward PI4KIIIα and PI4KIIIβ were selected. The homology modeling, molecular dynamic (MD) simulations [40-43] and binding free energy calculations [44-49] are combined to study the interaction mechanism of these compounds with PI4KIIIα and PI4KIIIβ. This paper is organized as follows. Section 2 presents the calculated results and discussions. In section 3, detailed descriptions of the computational methods used in this study are provided. Finally, a brief summary is given in section 4 .

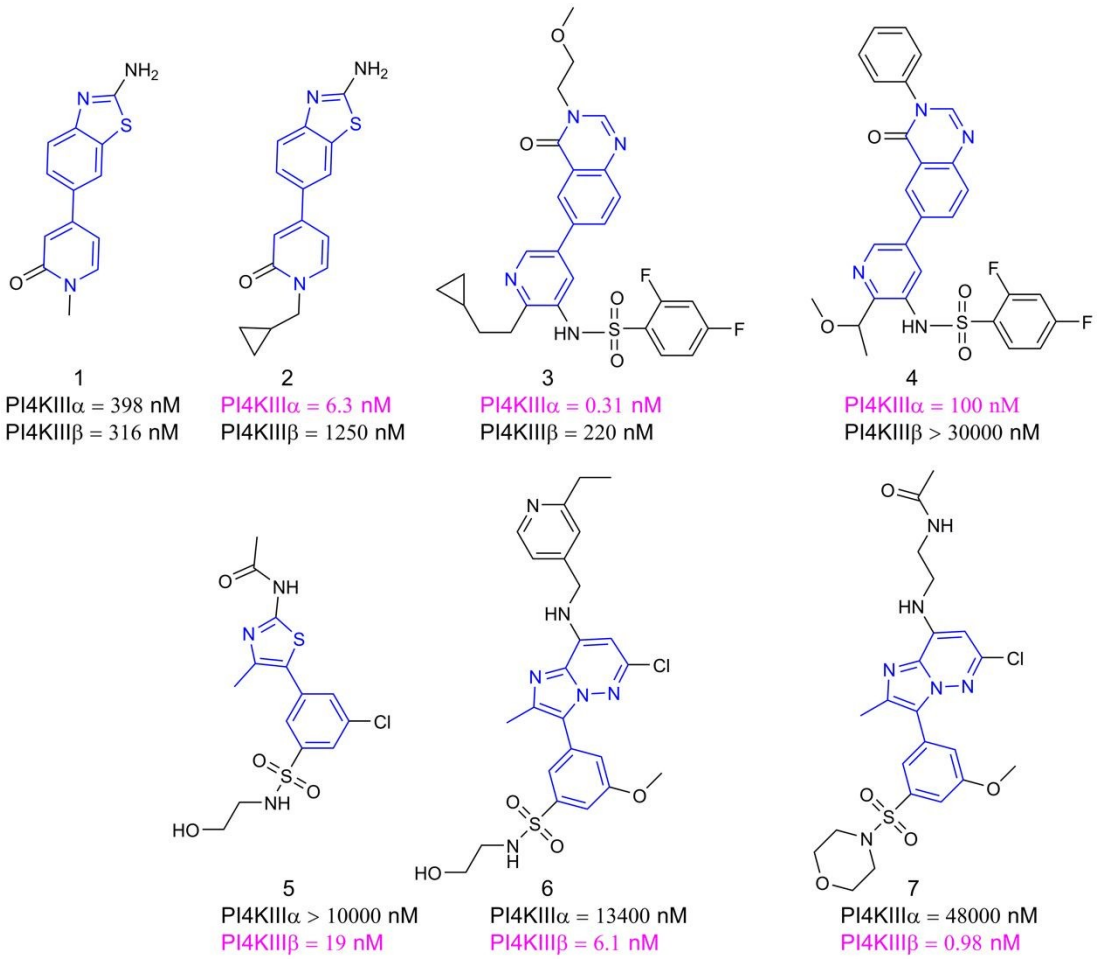

Figure 2. Molecular structures and IC50 values of seven inhibitors reported. Molecular skeleton marked with blue and selectivity marked with red.

Materials and Methods

Homology modeling and molecular docking

In this work, seven typical compounds with specific selectivity toward PI4KIIIα and

PI4KIIIβ were collected (Figure 2). The crystal structure of the catalysis domain of PI4KIIIβ (PDB ID: 4D0L) containing compound 5 [50] was used as a starting structure to construct the rest system with the others 6 compounds ((1, 2) [29], (3, 4) [22], and (6, 7) [35]) by docking them into the binding pocket of PI4KIIIβ. The residue sequence 1625 to 2042 of PI4KIIIα taken from the NCBI protein database (GenBank: AAC48730.1) [51] was used to generate the structure of the catalysis domain of PI4KIIIα by using the homology modelling technology with the I-TASSER approach [52-54]. During the preparation of the manuscript, one 3D structure of PI4KIIIα is determined by Lees et al. (PDB ID: 6BQ1) [55]. In order to check the quality of the homology model of PI4KIIIα, we aligned it with the experimental structure and the overall root mean square deviation (RMSD) of the backbone atoms is 2.14 Å. The RMSD of backbone atoms in the binding pocket of these two structures is only 1.68 Å, which illustrate the rationality of the homology modeling structure. Then the selected 7 compounds were docked into the binding pocket of PI4KIIIα. The molecular docking were performed by using the Glide module of the Schrodinger Suite 2014 [56-58].

In the crystal structure, the sulfonamide group of the compound 5 forms a strong hydrogen bond with the Lys549 residue of PI4KIIIβ[50]. As compounds 3-7 all have the sulfonamide group, only the binding poses in which this interaction was conserved were kept the pose clustering[59] was conducted (Table S1). The clusters obtained were ranked according to their average docking score. As shown in Figure S1, in 9 of the 14 systems, the binding pose with the highest docking score (lowest binding energy predicted by the scoring function) is in the most populated cluster. While in 12 of 14 systems, the binding pose with the lowest binding energy can be found in the cluster with the lowest binding energy. Therefore, it is reasonable to choose the binding pose which has the highest docking score for MD simulation. For the PI4KIIIα/3 system, the binding pose with the highest docking score was selected although it was clustered into the second class. While for the PI4KIIIβ/3 system, these is no binding pose which conserves the interaction between the sulfonamide group and Lys549, so we manually built the binding structure based on the selected binding pose of PI4KIIIβ/4 system.

Molecular dynamics simulations

To ensure the reliability of the calculated results, 3 individual MD simulation from the same initio structure were performed for each protein-ligand complex. All simulations were performed by using AMBER16 package [60]. The ff14SB force field was used to produce parameters for the protein [61]. The AM1-BCC atomic charges [62, 63] were assigned to each atom of ligands by using the Antechamber module [64]. The force field parameters of ligands were taken from the general AMBER force field (GAFF) [65]. Then each system was solvated in a truncated octahedral box of TIP3P [66] water molecules with a buffer distance of 12 Å and suitable counterions were added to neutralize the system. Before performing MD simulations, all systems were minimized using 3000 cycles of the steepest descent algorithm followed by 5000 cycles of the conjugate gradient algorithm to remove bad contacts generated in the initialization step. After minimization, each system was heated from 0 to 300K during 500 ps in an NVT

View Article Online
DOI: 10.1039/C9CP03598B

ensemble and then further equilibrated for 500 ps in an NPT ensemble. Finally, 60ns MD simulations were performed under the NPT ensemble. During MD simulation, the integral time step was set to 2fs, and the temperature was kept at 300K by using the Langevin dynamics [67] with a collision frequency of 1ps^{-1} and a constant pressure of 1 atm. The Particle Mesh Ewald(PME) method [68] was employed for treating the long-range electrostatics interactions, and the van der Waals interactions were truncated at 10 Å. Moreover, the SHAKE algorithm [69] was used to constrain all bonds involving hydrogen atoms.

Calculation of binding free energies based on MM/GBSA

Molecular dynamic simulations were conducted to generate a representative ensemble of structures, and MM/GBSA method was then used to calculate binding free energies of the complexes, this method can be conceptually summarized as the following

$$\Delta G_{bind} = G_{complex} - G_{protein} - G_{ligand} \quad (1)$$

where the binding free energy (ΔG_{bind}) is computed as the difference between the free energies of the complex ($G_{complex}$), the protein($G_{protein}$) and the ligand(G_{ligand}). The binding free energy is the sum of the following four terms:

$$\Delta G_{bind} = \Delta E_{ele} + \Delta E_{vdw} + \Delta G_{gb} + \Delta G_{np} - T\Delta S \quad (2)$$

in which $-T\Delta S$ denotes the conformational entropy was calculated by using the NMODE module [70] in AMBER16. The ΔE_{ele} is electrostatic interaction energy and ΔE_{vdw} is van der Waals interaction energy, representing the internal free energy of molecular mechanics in the gas. The solvation energy includes polar contribution ΔG_{gb} and non-polar contribution ΔG_{np}. ΔG_{gb} is computed by Generalized Born (GB) method [71], while the non-polar solvation energy ΔG_{np} was calculated by the solvent-accessible surface area (SASA) using the MSMS program [72] based on the equation 3

$$\Delta G_{np} = \gamma SASA + \beta \quad (3)$$

where the surface tension γ and offset β are empirical constants and set to 0.00542 kcal/(mol·Å^2) and 0.92 kcal/mol, respectively.

For each system, 500 snapshots were retrieved from the last 20 ns of MD trajectory with an interval of 40 ps. According to the MM/GBSA methods, the arithmetic averages of the internal energies and solvation free energies for each species in the equation 2 were computed based on this conformational ensemble. The calculation of entropy term ($-T\Delta S$) using the NMODE was time-consuming. Thus only 100 snapshots taken from in the last 20 ns of trajectories with an interval of 200 ps were applied to compute averaged entropic contribution to the binding free energy. To evaluate the contribution of specific residues to binding free

energies, residue-based free energy decomposition method was adopted to calculate ligand-residue interaction spectrum by using the same snapshots as those used in the binding free energy calculations [44].

There are five GB models named as GB^{HCT},[73] GB^{OBC}, GB^{OBC2},[74] GB^{NECK},[75] GB^{NECK2}.[76] can be used in the AMBER16 software, and each of them has one recommended atomic radii set (*mbondi* in GB^{HCT} (igb=1), *mbondi2* in GB^{OBC} (igb=2) and GB^{OBC2}(igb=5), *bondi* in GB^{NECK} (igb=7), and *mbondi3* in GB^{NECK2}(igb=8)). For comparison, all of these five GB models were used in the calculation.

Calculation of binding free energies based on MM/PBSA and QM-MM/GBSA

Although the MM/GBSA method had been proven to be a cost-effective method for the estimation of relative binding free energy[77, 78], to demonstrate the prediction capabilities in this study, we also employed the MM/PBSA and QM-MM/GBSA methods to evaluate the binding affinities. The algorithms of MM/PBSA and QM-MM/GBSA are similar to that of MM/GBSA, except that the Poisson–Boltzmann model is used to calculate the polar solvation free energy in MM/PBSA and the semi-empirical QM calculation is used to calculate the interaction energy between protein and ligand in the QM-MM/GBSA.

For comparison, 5 different atomic radii sets (*bondi, mbondi, mbondi2, mbondi3,* and *amber6*) were tested in the MM/PBSA calculation. In the QM-MM/GBSA calculations, the parameterized model number 6 (PM6)[79] semiempirical QM model (including PM6, PM6D, and PM6-DH+) was employed with different GB models. For the complex system contain compound 2-7, the ligand and five neighboring PI4KIIIα residues (Met1736, Ile1789, Tyr1825, Met1905 and Ile1915), five equivalent PI4KIIIβ residues (Leu374, Ile547, Tyr583, Leu663, and Ile673) were assigned to the QM zone. In the complex systems contain compound 1, the ligand and five neighboring PI4KIIIα residues (Lys1791, Cys1839, Ile1840, Met1905, and Ile1915), five equivalent PI4KIIIβ residues (Lys549, Pro597, Val598, Leu663, and Ile673) were assigned to the QM zone.

Results and Discussion

Binding free energy calculations

To evaluate binding affinities of different compounds with PI4KIIIα and PI4KIIIβ, MM/GBSA, MM/PBSA, and QM-MM/GBSA methods were applied to compute binding free energies of all complexes, and the results were listed in Table 1 (Table S2-S39, FigureS2-6.). From this large amount of data, one can find that, first of all, for each protein-ligand complex, the calculated binding enthalpies of 3 replicas agree very well with each other, which reflect the rationality of the MD simulations. Secondly, the relative free energies calculated by these three methods with different parameters are also consistent with each other. Therefore, to save the computational cost, entropy calculations were only performed for the first replica, and the following analysis are all based on this replica. In addition, it is important to note that we are more concerned with relative binding free energies instead of absolute binding free energies of each compound. As the MM/GBSA had been proven to be a cost-effective method for the estimation of relative binding free energy[77, 78] and its results are consistent with that of MM/PBSA and QM-MM/GBSA, thus only the results of the MM/GBSA (with the default GB

View Article Online
DOI: 10.1039/C9CP03598B

model, igb=5) are discussed in the flowing. As can be seen from the results, the calculations correctly yield the selectivity of seven compounds toward PI4KIIIα and PI4KIIIβ, which is in good agreement with the experimental IC50 values. The binding free energies of PI4KIIIα/1 complex (-18.19 kcal/mol) and PI4KIIIβ/1 complex (-18.82 kcal/mol) are approximately equal, which basically agrees with the experimental result that compound 1 is less selective between PI4KIIIα and PI4KIIIβ.

Binding free energies of the other systems obviously indicate that compounds 2, 3, and 4 prefer to bind to PI4KIIIα, while compounds 5, 6, and 7 prefer to bind to PI4KIIIβ. The currently calculated selectivity of these six compounds is also consistent with that determined by the experiments.

Table 1. The binding free energies of the PI4KIIIα and PI4KIIIβ complexes and the corresponding energy components[a] calculated by MM/GBSA (igb=5).

Compound	Subtype of PI4kIII	ΔE_{vdw}	ΔE_{ele}	ΔG_{gb}	ΔG_{np}	ΔH	$T\Delta S$	ΔG_{bind} [b]
1	α	-31.00	-22.64	24.31	-4.43	-33.76	-15.57	**-18.19**
	β	-35.69	-27.73	34.83	-4.39	-32.99	-14.17	**-18.82**
2	α	-45.52	-47.41	49.95	-6.07	-49.04	-15.47	**-33.57**
	β	-32.03	-45.39	50.36	-4.28	-31.34	-14.70	**-16.64**
3	α	-66.35	-35.91	52.27	-8.77	-58.77	-20.52	**-38.25**
	β	-47.2	-42.86	59.04	-6.21	-37.23	-19.51	**-17.72**
4	α	-60.00	-24.46	46.59	-7.85	-45.73	-19.99	**-25.74**
	β	-49.01	-25.27	44.10	-5.93	-36.10	-17.56	**-18.54**
5	α	-41.37	-40.70	50.60	-5.88	-37.34	-19.54	**-17.80**
	β	-42.77	-60.24	61.01	-5.65	-47.65	-13.92	**-33.73**
6	α	-48.85	-42.49	53.99	-6.95	-44.30	-21.39	**-22.91**
	β	-60.84	-66.30	74.09	-7.75	-60.80	-17.17	**-43.63**
7	α	-41.78	-17.33	30.99	-5.49	-33.60	-18.20	**-15.40**
	β	-58.24	-57.72	64.69	-7.05	-58.33	-17.33	**-41.00**

[a]All values are in kcal/mol.

[b] $\Delta G_{bind} = \Delta E_{ele} + \Delta E_{vdw} + \Delta G_{gb} + \Delta G_{np} - T\Delta S$.

Binding modes of the non-selective compound 1.

As shown in Figure 3, compound 1 is buried in the hydrophobic cleft of PI4KIIIα and PI4KIIIβ respectively and their binding modes are similar to each other. Structurally, compound 1 forms one hydrogen bonds with the backbone of residue Ile1840 in PI4KIIIα and two hydrogen bonds with the equivalent residue Val598 in PI4KIIIβ (Table S40). These two residues produce the strongest favorable interactions with the compound 1 in the PI4IKIIIα/1 and PI4KIIIβ/1 complex, respectively (Figure 4). Interestingly, during MD simulation, compound 1 forms a stable hydrogen bond with Lys1791 in PI4KIIIα, but there is no hydrogen bond formed between compound 1 and the equivalent Lys549 residue in PI4KIIIβ (Table S40). As shown in Figure 4, Lys1791 contributes -2.32 kcal/mol to the binding while the contribution of Lys549 is +0.02 kcal/mol. It should be mentioned that there are three residues in PI4KIIIβ, Tyr673, Ile595, and

Ile547, contribute ~-2.6, -1.9, and -1.8 kcal/mol to the binding with compound 1, respectively. However, the corresponding three residues in PI4KIIIα, Tyr1915, Ile1837, and Ile1789, only contribute -1.6, -1.0 and -1.2 kcal/mol to the interaction (Figure 4). In summary, although compound 1 forms one more hydrogen bond with PI4KIIIα, its binding ability with PI4KIIIβ is still slightly stronger. However, the difference in the binding affinity is relatively very small, so we cannot observe obvious selectivity of this compound toward PI4KIIIα and PI4KIIIβ.

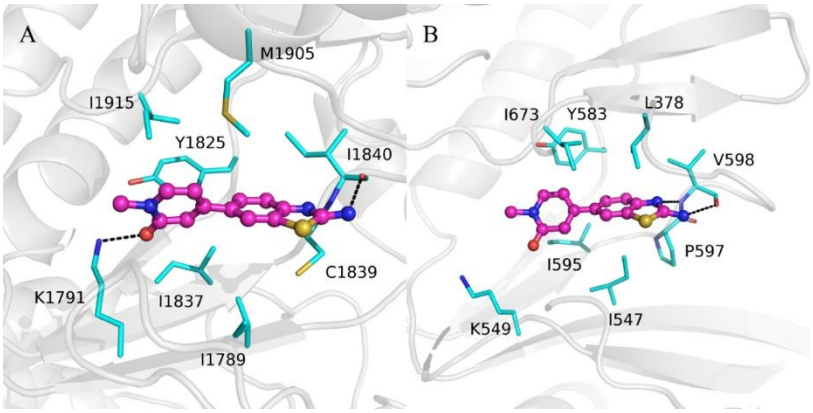

Figure 3. Binding modes of compound 1 relative to key residues in PI4KIIIα and PI4KIIIβ: (A) PI4KIIIα /1 complex. (B) PI4KIIIβ/1 complex.

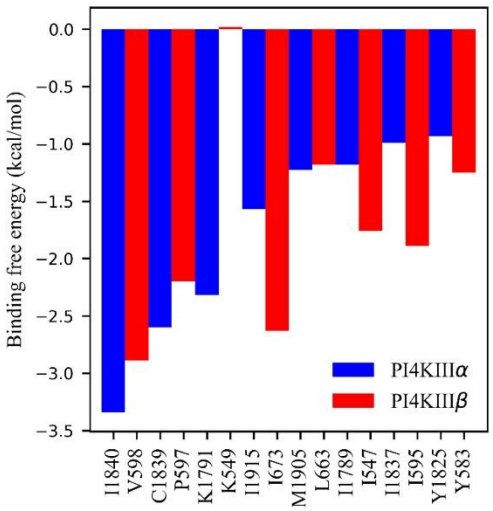

Figure 4. Residue-specific binding free energies of compound 1 to PI4KIIIα and PI4KIIIβ from MM/GBSA calculations.

High selectivity of the compounds 2, 3, and 4 toward PI4KIIIα over PI4KIIIβ

Compared with compound 1, the compound 2 only has one more cyclopropane moiety but shows stronger selectivity toward PI4KIIIα than PI4KIIIβ. There is a sub-pocket (denoted as sub-pocket A for convenience) build by four residues in PI4KIIIα: Val1827, Cys1796, Asp1799 and Lys1791. Similar to PI4KIIIα, the four equivalent residues in PI4KIIIβ, including Ile585, Leu554, Glu557 and Lys549, also form a sub-pocket (sub-pocket B). We can see that the side-chains of the four residues in sub-pocket A are shorter than that in sub-pocket B. As a result, the volume of the sub-pocket A is bigger than sub-pocket B. Thus the sub-pocket A is large enough

to accommodate the cyclopropane moiety of compound 2, which is agree with the experiment [29]. As shown in Figure 5A, 5B and Table S40, an oxygen atom of the compound forms a hydrogen bond with Lys1791 in PI4KIIIα and Lys549 inPI4KIIIβ. However, the free energy donated by Lys1791 is -2.35 kcal/mol, while Lys549 only contributes -1.39 kcal/mol to the binding, this may be because the space barrier of the relatively smaller sub-pocket B. Totally, sub-pocket A contributes about -2.73 kcal/mol for the binding of the compound 2, while the contribution from sub-pocket B is even a positive value (0.53 kcal/mol).

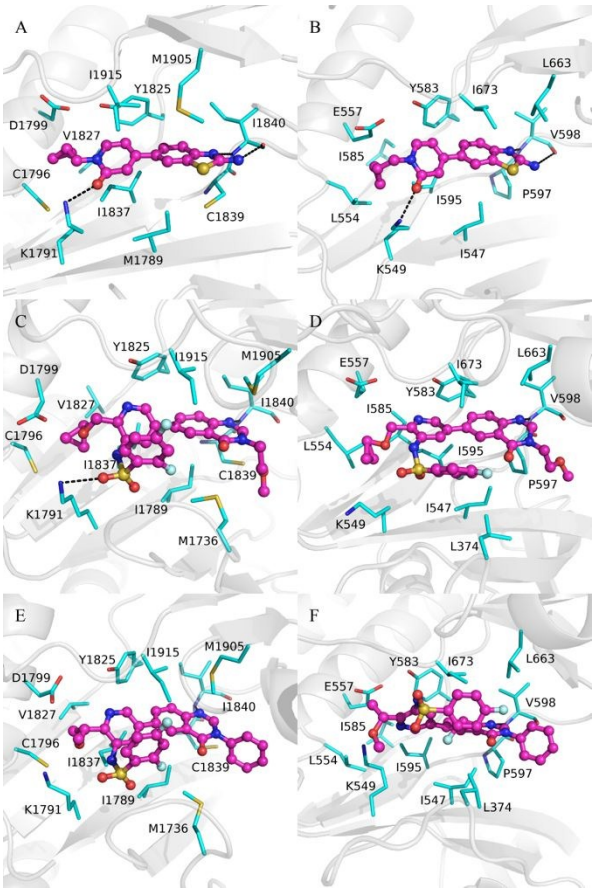

Figure 5. Binding modes of the compound 2, 3, and 4 relative to key residues in PI4KIIIα and PI4KIIIβ: (A) PI4KIIIα/2 complex, (B) PI4KIIIβ/2 complex, (C) PI4KIIIα/3 complex, (D) PI4KIIIβ/3 complex, (E) PI4KIIIα /4 complex, and (F) PI4KIIIβ/4 complex.

Both residue Ile1840 and its equivalent residue Val598 form two hydrogen bonds with compound 2. However, as shown in Figure 6A, the interaction energy of Ile1840 with compound 2 is -3.20 kcal/mol, which is stronger than that of Val598 (-2.66 kcal/mol). In addition, Cys1839 and Met1905 in PI4KIIIα also contribute more interaction energies (-2.97 and -1.11 kcal/mol) than their equivalent residues Pro597 and Leu663 (-2.19 and -0.68 kcal/mol) to the binding. The above analyses explain the stronger binding affinity of compound 2 to PI4KIIIα over PI4KIIIβ.

View Article Online
DOI: 10.1039/C9CP03598B

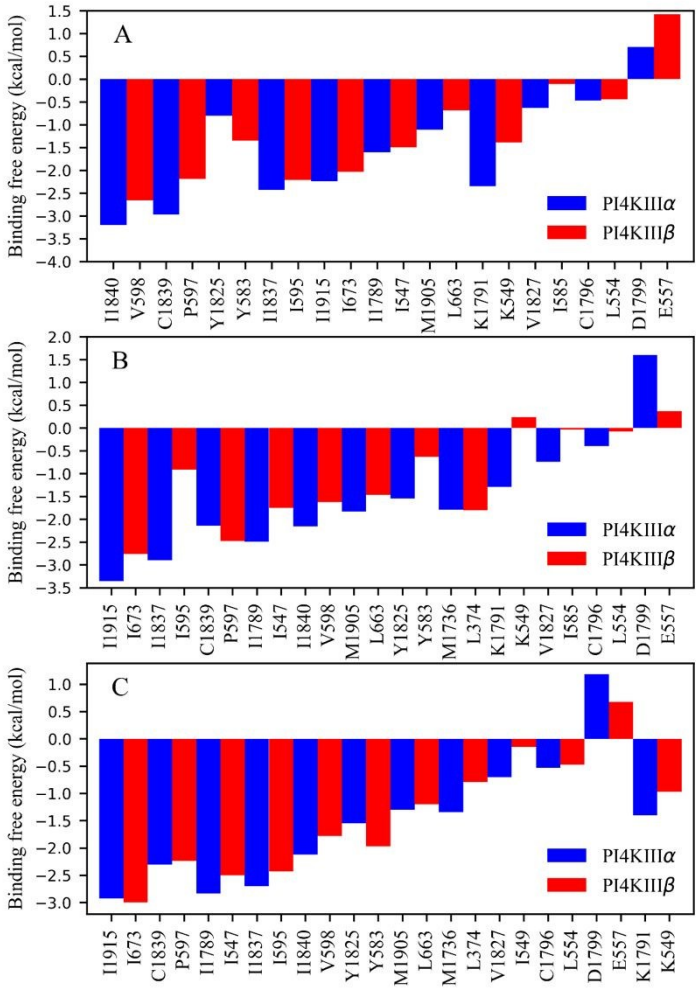

Figure 6. Residue-specific binding free energies of top residues in PI4KIIIα and PI4KIIIβ to the compound 2, 3, and 4: (A) the compound 2, (B) the compound 3, and (C) the compound 4.

Similar to compound 2, compound 3 also has a cyclopropane moiety which is buried more deeply in the sub-pocket A than in the sub-pocket B (Figure 5C and 5D). The sulfonamide moiety of compound 3 forms a hydrogen bond with Lys1791 in PI4KIIIα, while the cyclopropane moiety pushes the equivalent residue Lys549 away from the sub-pocket B and thus loses this hydrogen bond (Table S40). As shown in Figure 6B, Lys1791 contributes more energy (-1.29 kcal/mol) to the binding with compound 3 than Lys549 (0.24 kcal/mol). It is worth to mention that residue Asp1799 in sub-pocket A contributes an unfavorable interaction energy of 1.60 kcal/mol, which is larger than that of Glu557 (0.37 kcal/mol) in sub-pocket B. However, the total contribution from sub-pocket A to the binding is -0.82 kcal/mol, which is stronger than that of sub-pocket B (0.50 kcal/mol).

Compound 3 also forms two hydrogen bonds with Ile1840 in PI4KIIIα and Val598 in PI4KIIIβ. However, its interaction with Ile1840 is strengthened by 0.5 kcal/mol compared to that of residue Val598. In addition, hydrophobic residues Ile1837, Ile1915 and Tyr1825 in PI4KIIIα also contribute stronger interactions with compound 3 than their equivalent residues Ile595, Ile673 and Tyr583 in PI4KIIIβ. All the above results show that compound 3 has the stronger binding ability with PI4KIIIα than PI4KIIIβ.

As shown in Figure 2, compound 4 has the same molecular skeleton as compound 3. According to Figure 5E and 5F, the methoxyethyl group of compound 4 exhibited different binding poses between PI4KIIIα and PI4KIIIβ. The methyl group at the end of the methoxyethyl group is buried into the sub-pocket A deeply and the remained methoxy group toward the outside of the binding pocket (Figure 5E). Under these circumstances, the sub-pocket A contributes a net favorable binding free energy of ~-1.50 kcal/mol. Due to the electrostatic repulsion, Asp1799 in PI4KIIIα gives the unfavorable binding free energy of ~1.2 kcal/mol (Figure 6C). Three residues Lys1791, Cys1796, and Val1827 in sub-pocket A contribute of -1.4, -0.5, and -0.7 kcal/mol to the binding, respectively. However, In the PI4KIIβ/4 complex, the entire methoxyethyl group does not enter the sub-pocket B. Although residue Lys549 in PI4KIIIβ can form a hydrogen bond with the sulfonamide moiety of compound 4 occasionally, the hydrogen bond occupancy is only 17.4%. Four residues Lys549, Leu554, Glu557, and Ile585 in sub-pocket B contributes ~-1.0, -0.3, +0.7, and -0.2 kcal/mol to the binding (Figure 6C), respectively. The sub-pocket A not only gives a favorable binding free energy but also accommodates a large part of the methoxyethyl group. Thus, the rest part of compound 4 has more opportunity to interact with other residues in the binding pocket. As shown in Figure 6C, five residues from PI4KIIIα, including Ile1840, Ile1789, Ile1837, Met1905 and Met1736, contribute -2.12, -2.83, -2.70, -1.30 and -1.34 kcal/mol to the binding, respectively. Compared with sub-pocket A, the methoxyethyl group cannot enter sub-pocket B at all, and it cannot form any strong interaction with other residues in the binding pocket. Affected by the steric hindrance of the methoxyethyl group, the rest part of compound 4 also cannot form strong interaction with the binding pocket. Five equivalnet residues Val598, Ile547, Ile595, Leu663 and Leu374 in PI4KIIIβ only contribute -1.78, -2.50, -2.43, -1.20 and -0.79 kcal/mol to the binding. From the above results, it can be found that the compound 4 prefers to bind with PI4KIIIα instead of PI4KIIIβ.

In summary, compounds 1, 2, 3, and 4 have similar molecular skeleton (Figure 1). Compound 1 is relatively small so that it can bind to PI4KIIIα and PI4KIIIβ with nearly the same mode. Compounds 2, 3, and 4 have a branched chain (the cyclopropane moiety in compounds 2 and 3, and the methoxyethyl group in compound 4) which extends into a sub-pocket in the binding point. The sub-pocket in PI4KIIIα is obviously bigger than that in PI4KIIIβ, thus it provides a better help in the interaction with these three molecules in two ways. Firstly, compared with the sub-pocket in PI4KIIIβ, it provides more favorable interactions with the cyclopropane moiety in compound 2, and 3. Secondly, it gives the rest part of compound 4 more opportunity to interact with other residues in the binding pocket.

High selectivity of the compounds 5, 6, and 7 toward PI4KIIIβ over PI4KIIIα

As shown in Figure 7, the binding modes of compound 5 with PI4KIIIα and PI4KIIIβ are different with each other. This compound forms two hydrogen bonds with residue Val598 in PI4KIIIβ, but there is no corresponding hydrogen bond formed between it and the residue Ile1840 in PI4KIIIα. Finally, Val598 donates -3.64 kcal/mol to the binding free energy, its neighboring residue Pro597 also donates -2.10 kcal/mol, while the corresponding residues Ile1840 and Cys1839 only contribute -1.97 and -1.80 kcal/mol, respectively (Figure 8A). In addition, one oxygen atom of the sulfonamide moiety in the compound 5 forms a hydrogen bond with residue Lys1791 in PI4KIIIα and the corresponding residue Lys549 in PI4KIIIβ (Figure

7A and 7B, Table S40). However, the hydrogen bond occupancy with Lys1791 is only 14.1%, while the occupancy with Lys549 is 97.2%. The binding free energy contribute by residue Lys1791 (-2.17 kcal/mol) is less than that of residue Lys549 (-3.01 kcal/mol). Moreover, residue Tyr1825 in PI4KIIIα only contributes -1.09 kcal/mol to the binding, but the corresponding residue Tyr583 in PI4KIIIβ offer -1.92 kcal/mol. Those free energy differences confirmed that compound 5 binding tighter with PI4KIIIβ than PI4KIIIα.

Obvious differences can be found between the binding modes of compound 6 with PI4KIIIα and PI4KIIIβ (Figure 7C, 7D). The ethylpridine group of compound 6 conducts a π-π interaction with Tyr1744 in PI4KIIIα, which contributes -1.07 kcal/mol to the binding, while the corresponding residue Leu383 in PI4KIIIβ contributes -0.96 kcal/mol (Figure 8B). The oxygen atom of sulfonamide moiety in compound 6 forms a hydrogen bond with Lys1791 in PI4KIIIα and Lys549 in PI4KIIIβ, respectively. However, the contribution of Lys549 to the binding free energy is 0.88 kcal/mol more than that of Lys1791. Compound 6 also forms three hydrogen bonds with Val598 and Asn600 in PI4KIIIβ (the contribution to the binding are -2.25, and -0.92 kcal/mol, respectively), which further strengthen their interaction. In contrary, their corresponding residues in PI4KIIIα interact very week with compound 6, the contribution of residue Ile1840, and Asp1842 to the binding are only -0.49 and -0.05 kcal/mol, respectively. In addition, residue Tyr583 at the end of the pocket has a favorable free energy contribution of -1.65 kcal/mol. However, the contribution of Tyr1825 is only -0.42 kcal/mol. These results give a clear indication that the compound 6 has higher selectivity toward PI4KIIIβ over PI4KIIIα.

Figure 7E and 7F depict the binding modes of compound 7 with PI4KIIIα and PI4KIIIβ. As can be seen, compound 7 forms two hydrogen bonds with residue Val598 in PI4KIIIβ (Table S40). Furthermore, the carbonyl oxygen atom of the N-ethylacetamide group in the compound 7 also forms a hydrogen bond with the amide hydrogen atom of residue Asn600. However, in the PI4KIIIα/7 complex, compound 7 does not form these hydrogen bonds. Instead, the N-ethylacetamide group of compound 7 is toward outside the pocket. According to Figure 8C, three residues in PI4KIIIβ, including Pro597, Val598 and Val599, provide favorable energy contributions ranging from -2.01 to -2.60 kcal/mol for the binding of compound 7. However, their three equivalent residues Cys1839, Ile1840 and Pro1841 in PI4KIIIα only contribute -0.06, -0.16, 0.01 kcal/mol to the binding. Lys549 of PI4KIIIβ generate hydrogen bonding interactions with the oxygen atom in sulfonamide moiety of compound 7, but this hydrogen bond was not found in PI4KIIIα. As we can found that residue Lys1791 only contributes -1.22 kcal/mol to the binding, while Lys549 contributes -3.34 kcal/mol. In addition, residue Tyr583 in PI4KIIIβ provides binding free energy of -1.81 kcal/mol, but its equivalent residue Tyr1825 in PI4KIIIα only produces -0.14 kcal/mol. According to those analysis, it is concluded that the compound 7 has higher selectivity toward PI4KIIIβ than PI4KIIIα.

View Article Online
DOI: 10.1039/C9CP03598B

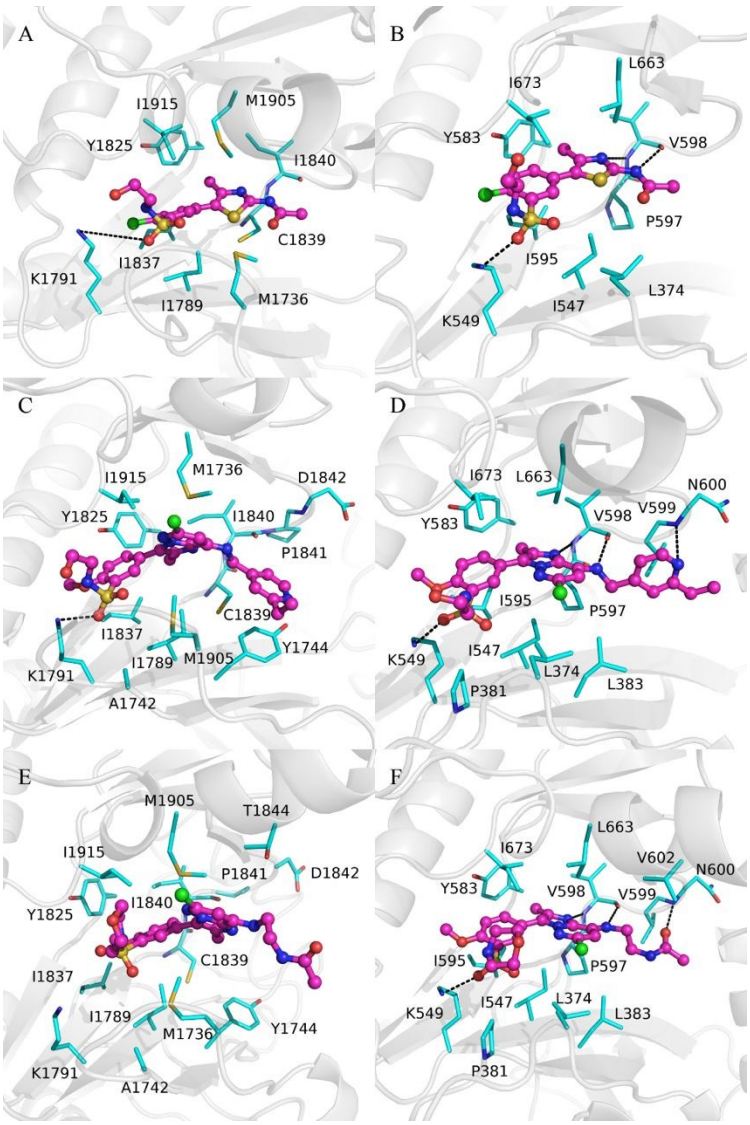

Figure 7. Binding modes of the compound 5, 6, and 7 relative to key residues in , in PI4KIIIα and PI4KIIIβ: (A) PI4KIIIα /5 complex, (B) PI4KIIIβ/5 complex, (C) PI4KIIIα /6 complex, (D) PI4KIIIβ/6 complex, (E) PI4KIIIα /7 complex, and (F) PI4KIIIβ/7 complex.

Through careful examination of three-dimensional binding modes of compound 7 with PI4KIIIα and PI4KIIIβ, it is found that residues Ile1840 and Cys1839 in PI4KIIIα have larger side chain than their equivalent residues Val598 and Pro597 in PI4KIIIβ. Meanwhile, compounds 5, 6, and 7 all have one 6-chloro-2-methylimidazo[1,2-b]pyridazine group on the molecular skeleton. It seems that the relative larger residues I1840 and Cys1839 make the binding pocket in PI4KIIIα too narrow to adopt the 6-chloro-2-methylimidazo[1,2-b]pyridazine group. Instead, the binding pocket at the same location of PI4KIIIβ is wider than that of PI4KIIIα, thus it is easier for PI4KIIIβ to accept those three compounds and form move favorable interactions.

View Article Online
DOI: 10.1039/C9CP03598B

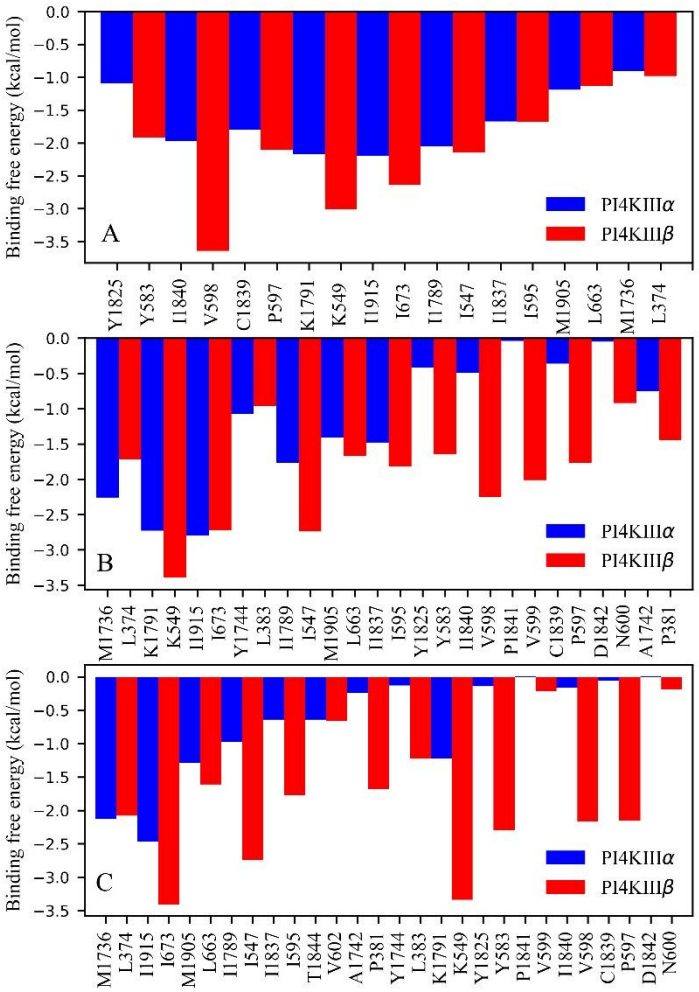

Figure 8. Residue-specific binding free energies of top residues in PI4KIIIα and PI4KIIIβ to the compounds 5, 6 and 7: (A) the compound 5, (B) the compound 6, and (C) the compound 7.

Conclusions

In this study, MD simulation and the MM/GBSA method are combined to study the interaction of 7 compounds toward the PI4KIIIα and PI4KIIIβ enzymes. The calculated binding free energies based on MD trajectories prove that compounds 2, 3, and 4 have higher binding affinity to PI4KIIIα over PI4KIIIβ, while compounds 5, 6, and 7 prefer to bind with PI4KIIIβ than PI4KIIIα. Meanwhile, the compound 1 does not generate a distinct difference in selectivity toward PI4KIIIα and PI4KIIIβ. These results are consistent with the experimental measurements.

The residue-based free energy decomposition was applied to further explore the origin of the selectivity of these compounds at the atomic level. The results show that the cyclopropane group in compounds 2, 3, and the methoxyethyl group in compound 4 are extend into a sub-pocket in the binding point. The sub-pocket in PI4KIIIα composed by residue Val1827, Cys1796, Asp1799 and Lys1791 is obviously bigger than the sub-pocket in PI4KIIIβ which is composed by Ile585, Leu554, Glu557 and Lys549. Thus, compared with PI4KIIIβ, PI4KIIIα provides more favorable interactions with the cyclopropane moiety in compound 2, and 3. In addition, although its interaction with the methoxyethyl group in compound 4 is unfavorable, it

gives the rest part of compound 4 more opportunity to interact with other residues in the binding pocket. On the other hand, it is found that residues Ile1840 and Cys1839 in PI4KIIIα have larger side chain than their equivalent residues Val598 and Pro597 in PI4KIIIβ. Meanwhile, compounds 5, 6, and 7 all have one 6-chloro-2-methylimidazo[1,2-b]pyridazine group on the molecular skeleton. The relative larger residues Ile1840 and Cys1839 make the binding pocket in PI4KIIIα too narrow to adopt the 6-chloro-2-methylimidazo[1,2-b] pyridazine group. Instead, the binding pocket at the same location in PI4KIIIβ is wider compared to PI4KIIIα, thus it is easier for PI4KIIIβ to accept those three compounds and form move favorable interactions.

It is expected that detailed binding information found in this study can provide useful help for the structure-based design of selective inhibitors toward PI4KIIIα and PI4KIIIβ.

Author Contributions: Shuaizhen Tian and Xiao Liu performed the MD simulations, drafted the main text of the manuscript and prepared all the figures; Jinzhe Zeng and Jianzhong Chen helped with data analysis and revised the manuscript; John ZH Zhang and Tong Zhu designed this study.

Funding: This work was supported by the Ministry of Science and Technology of China (Grant No. 2016YFA0501700), the National Natural Science Foundation of China (Grants No.91641116, and 11504206), Innovation Program of Shanghai Municipal Education Commission (201701070005E00020) and NYU Global Seed Grant.

Acknowledgments: We thank the ECNU Multifunctional Platform for Innovation (001) for providing us with computer time.

Conflicts of interest: The authors declare no conflict of interest.

View Article Online
DOI: 10.1039/C9CP03598B

References

1. H. J. McCrea and P. De Camilli, *Physiology*, 2009, **24**, 8-16.
2. G. R. Hammond, M. J. Fischer, K. E. Anderson, J. Holdich, A. Koteci, T. Balla and R. F. Irvine, *Sci*, 2012, **337**, 727-730.
3. J. Tan and J. A. Brill, *Crit. Rev. biochem. Mol. Biol.*, 2014, **49**, 33-58.
4. F. H. Santiago-Tirado and A. Bretscher, *Trends Cell Biol.*, 2011, **21**, 515-525.
5. G. D'Angelo, M. Vicinanza, A. Di Campli and M. A. De Matteis, *J. Cell Sci.*, 2008, **121**, 1955-1963.
6. G. D'Angelo, M. Vicinanza, C. Wilson and M. A. De Matteis, *Subcell Biochem*, 2012, **59**, 255-270.
7. K. L. Berger, J. D. Cooper, N. S. Heaton, R. Yoon, T. E. Oakland, T. X. Jordan, G. Mateu, A. Grakoui and G. Randall, *Proc. Natl. Acad. Sci. U. S. A.*, 2009, **106**, 7577-7582.
8. J. Borawski, P. Troke, X. Puyang, V. Gibaja, S. Zhao, C. Mickanin, J. Leighton-Davies, C. J. Wilson, V. Myer and I. CornellaTaracido, *J. Virol.*, 2009, **83**, 10058-10074.
9. F. H. Vaillancourt, L. Pilote, M. Cartier, J. Lippens, M. Liuzzi, R. C. Bethell, M. G. Cordingley and G. Kukolj, *Virology*, 2009, **387**, 5-10.
10. A. W. Tai, Y. Benita, L. F. Peng, S.-S. Kim, N. Sakamoto, R. J. Xavier and R. T. Chung, *Cell Host Microbe*, 2009, **5**, 298-307.
11. M. Trotard, C. Lepère-Douard, M. Régeard, C. Piquet-Pellorce, D. Lavillette, F.-L. Cosset, P. Gripon and J. Le Seyec, *FASEB J.*, 2009, **23**, 3780-3789.
12. E. Gower, C. Estes, S. Blach, K. Razavi-Shearer and H. Razavi, *J. Hepatol.*, 2014, **61**, S45-S57.
13. S. Reiss, I. Rebhan, P. Backes, I. Romero-Brey, H. Erfle, P. Matula, L. Kaderali, M. Poenisch, H. Blankenburg and M.-S. Hiet, *Cell Host Microbe*, 2011, **9**, 32-45.
14. S. Reiss, C. Harak, I. Romero-Brey, D. Radujkovic, R. Klein, A. Ruggieri, I. Rebhan, R. Bartenschlager and V. Lohmann, *PLoS Pathog.*, 2013, **9**, e1003359.
15. K. Wong, R. Meyers and L. C. Cantley, *J. Biol. Chem.*, 1997, **272**, 13236-13241.
16. A. Godi, P. Pertile, R. Meyers, P. Marra, G. Di Tullio, C. Iurisci, A. Luini, D. Corda and M. A. De Matteis, *Nat. Cell Biol.*, 1999, **1**, 280-287.
17. N.-Y. Hsu, O. Ilnytska, G. Belov, M. Santiana, Y.-H. Chen, P. M. Takvorian, C. Pau, H. van der Schaar, N. Kaushik-Basu and T. Balla, *Cell*, 2010, **141**, 799-811.
18. N. Altan-Bonnet and T. Balla, *Trends. Biochem. Sci.*, 2012, **37**, 293-302.
19. C. Mello, E. Aguayo, M. Rodriguez, G. Lee, R. Jordan, T. Cihlar and G. Birkus, *Antimicrob. agents CH.*, 2014, **58**, 1546-1555.
20. H. M. Van Der Schaar, L. Van Der Linden, K. H. Lanke, J. R. Strating, G. Pürstinger, E. De Vries, C. A. De Haan, J. Neyts and F. J. Van Kuppeveld, *Cell Res.*, 2012, **22**, 1576-1592.
21. A. L. Greninger, G. M. Knudsen, M. Betegon, A. L. Burlingame and J. L. DeRisi, *J. Virol.*, 2012, **86**, 3605-3616.
22. S. Noji, N. Seki, T. Maeba, T. Sakai, E. Watanabe, K. Maeda, K. Fukushima, T. Noguchi, K. Ogawa and Y. Toyonaga, *ACS Med. Chem. Lett.*, 2016, **7**, 919-923.
23. A. Bianco, V. Reghellin, L. Donnici, S. Fenu, R. Alvarez, C. Baruffa, F. Peri, M. Pagani, S. Abrignani and P. Neddermann, *PLoS Pathog.*, 2012, **8**, e1002576.
24. U. Schmitz and S.-L. Tan, *Recent patents on anti-infective drug discovery*, 2008, **3**, 77-92.
25. A. L. Leivers, M. Tallant, J. B. Shotwell, S. Dickerson, M. R. Leivers, O. B. McDonald, J. Gobel, K. L. Creech, S. L. Strum and A. Mathis, *J. Med. Chem.*, 2013, **57**, 2091-2106.

26. C. Spickler, J. Lippens, M.-K. Laberge, S. Desmeules, É. Bellavance, M. Garneau, T. Guo, Q. Hucke, P. Leyssen and J. Neyts, *Antimicrob. Agents CH.*, 2013, **57**, 3358-3368.
27. M. J. LaMarche, J. Borawski, A. Bose, C. Capacci-Daniel, R. Colvin, M. Dennehy, J. Ding, M. Dobler, J. Drumm and L. A. Gaither, *Antimicrob. Agents CH.*, 2012, **56**, 5149-5156.
28. E. P. Keaney, M. Connolly, M. Dobler, R. Karki, A. Honda, S. Sokup, S. Karur, S. Britt, A. Patnaik and P. Raman, *Biorg. Med. Chem. Lett.*, 2014, **24**, 3714-3718.
29. M. J. Waring, D. M. Andrews, P. F. Faulder, V. Flemington, J. C. McKelvie, S. Maman, M. Preston, P. Raubo, G. R. Robb and K. Roberts, *Chem. Commun.*, 2014, **50**, 5388-5390.
30. B. Tóth, A. Balla, H. Ma, Z. A. Knight, K. M. Shokat and T. Balla, *J. Biol. Chem.*, 2006, **281**, 36369-36377.
31. A. Balla, G. Tuymetova, B. Toth, Z. Szentpetery, X. Zhao, Z. A. Knight, K. Shokat, P. J. Steinbach and T. Balla, *Biochemistry*, 2008, **47**, 1599-1607.
32. M. Arita, H. Kojima, T. Nagano, T. Okabe, T. Wakita and H. Shimizu, *J. Virol.*, 2011, **85**, 2364-2372.
33. I. Mejdrová, D. Chalupská, M. Kögler, M. Šála, P. Plačková, A. Baumlová, H. Hřebabecký, E. k. Procházková, M. Dejmek and R. m. Guillon, *J. Med. Chem.*, 2015, **58**, 3767-3793.
34. F. U. Rutaganira, M. L. Fowler, J. A. McPhail, M. A. Gelman, K. Nguyen, A. Xiong, G. L. Dornan, B. Tavshanjian, J. S. Glenn and K. M. Shokat, *J. Med. Chem.*, 2016, **59**, 1830-1839.
35. I. Mejdrová, D. Chalupská, P. Plačková, C. Müller, M. Šála, M. Klíma, A. Baumlová, H. Hrebabecky, E. Prochazkova and M. Dejmek, *J. Med. Chem.*, 2016, **60**, 100-118.
36. G. Powis, R. Bonjouklian, M. M. Berggren, A. Gallegos, R. Abraham, C. Ashendel, L. Zalkow, W. F. Matter, J. Dodge and G. Grindey, *Cancer Res.*, 1994, **54**, 2419-2423.
37. S. Nakanishi, K. J. Catt and T. Balla, *Proc. Natl. Acad. Sci. U. S. A.*, 1995, **92**, 5317-5321.
38. G. J. Downing, S. Kim, S. Nakanishi, K. J. Catt and T. Balla, *Biochemistry*, 1996, **35**, 3587-3594.
39. A. W. Tai, N. Bojjireddy and T. Balla, *Anal. Biochem.*, 2011, **417**, 97-102.
40. F. Yan, X. Liu, S. Zhang, J. Su, Q. Zhang and J. Chen, *Int. J. Mol. Sci.*, 2018, **19**, 2496.
41. G. Hu, X. Yu, Y. Bian, Z. Cao, S. Xu, L. Zhao, B. Ji, W. Wang and J. Wang, *Int. J. Mol. Sci.*, 2018, **19**, 3524.
42. Y. Gao, T. Zhu and J. Chen, *Chem. Phys. Lett.*, 2018, **706**, 400-408.
43. Q. Wang, X. An, J. Xu, Y. Wang, L. Liu, E. L.-H. Leung and X. Yao, *Org. Biomol. Chem.*, 2018, **16**, 6521-6530.
44. H. Gohlke, C. Kiel and D. A. Case, *J. Mol. Biol.*, 2003, **330**, 891-913.
45. H. Liu and X. Yao, *Mol. pharmaceut.*, 2009, **7**, 75-85.
46. Y.-L. Cui, Q.-C. Zheng, J.-L. Zhang, Q. Xue, Y. Wang and H.-X. Zhang, *J. Chem. Inf. Model.*, 2013, **53**, 3308-3317.
47. L. Chen, J.-L. Zhang, L.-Y. Yu, Q.-C. Zheng, W.-T. Chu, Q. Xue, H.-X. Zhang and C.-C. Sun, *J. Phys. Chem. B*, 2012, **116**, 12415-12425.
48. Y. Zhou, N. Zhang, W. Chen, L. Zhao and R. Zhong, *Phys. Chem. Chem. Phys.*, 2016, **18**, 9202-9210.
49. J. Chen, J. Wang and W. Zhu, *Phys. Chem. Chem. Phys.*, 2017, **19**, 3067-3075.
50. J. E. Burke, A. J. Inglis, O. Perisic, G. R. Masson, S. H. McLaughlin, F. Rutaganira, K. M. Shokat and R. L. Williams, *Science*, 2014, **344**, 1035-1038.
51. T. Balla, G. J. Downing, H. Jaffe, S. Kim, A. Zólyomi and K. J. Catt, *J. Biol. Chem.*, 1997, **272**,

View Article Online
DOI: 10.1039/C9CP03598B

18358-18366.

52. Y. Zhang, *BMC Bioinformatics*, 2008, **9**, 40.
53. A. Roy, A. Kucukural and Y. Zhang, *Nat. Protoc.*, 2010, **5**, 725-738.
54. J. Yang, R. Yan, A. Roy, D. Xu, J. Poisson and Y. Zhang, *Nat. Methods*, 2015, **12**, 7-8.
55. J. A. Lees, Y. Zhang, M. S. Oh, C. M. Schauder, X. Yu, J. M. Baskin, K. Dobbs, L. D. Notarangelo, P. De Camilli, T. Walz and K. M. Reinisch, *Proceedings of the National Academy of Sciences*, 2017, **114**, 13720-13725.
56. R. A. Friesner, R. B. Murphy, M. P. Repasky, L. L. Frye, J. R. Greenwood, T. A. Halgren, P. C. Sanschagrin and D. T. Mainz, *J. Med. Chem.*, 2006, **49**, 6177-6196.
57. R. A. Friesner, J. L. Banks, R. B. Murphy, T. A. Halgren, J. J. Klicic, D. T. Mainz, M. P. Repasky, E. H. Knoll, M. Shelley and J. K. Perry, *J. Med. Chem.*, 2004, **47**, 1739-1749.
58. T. A. Halgren, R. B. Murphy, R. A. Friesner, H. S. Beard, L. L. Frye, W. T. Pollard and J. L. Banks, *J. Med. Chem.*, 2004, **47**, 1750-1759.
59. S. Makeneni, D. F. Thieker and R. J. Woods, *Journal of chemical information and modeling*, 2018, **58**, 605-614.
60. R. M. B. D.A. Case, D.S. Cerutti, T.E. Cheatham, III, T.A. Darden, R.E. Duke, T.J. Giese, H. Gohlke, A.W. Goetz, N. Homeyer, S. Izadi, P. Janowski, J. Kaus, A. Kovalenko, T.S. Lee, S. LeGrand, P. Li, C. Lin, T. Luchko, R. Luo, B. Madej, D. Mermelstein, K.M. Merz, G. Monard, H. Nguyen, H.T. Nguyen, I. Omelyan, A. Onufriev, D.R. Roe, A. Roitberg, C. Sagui, C.L. Simmerling, W.M. Botello-Smith, J. Swails, R.C. Walker, J. Wang, R.M. Wolf, X. Wu, L. Xiao and P.A. Kollman. , *University of California, San Francisco*, 2016.
61. J. A. Maier, C. Martinez, K. Kasavajhala, L. Wickstrom, K. E. Hauser and C. Simmerling, *J. Chem. Theory. Comput.*, 2015, **11**, 3696-3713.
62. A. Jakalian, B. L. Bush, D. B. Jack and C. I. Bayly, *J. Comput. Chem.*, 2000, **21**, 132-146.
63. A. Jakalian, D. B. Jack and C. I. Bayly, *J. Comput. Chem.*, 2002, **23**, 1623-1641.
64. J. Wang and P. A. Kollman, *J. Comput. Chem.*, 2001, **22**, 1219-1228.
65. J. Wang, R. M. Wolf, J. W. Caldwell, P. A. Kollman and D. A. Case, *J. Comput. Chem.*, 2004, **25**, 1157-1174.
66. W. L. Jorgensen, J. Chandrasekhar, J. D. Madura, R. W. Impey and M. L. Klein, *J. Chem. Phys.*, 1983, **79**, 926-935.
67. R. W. Pastor, B. R. Brooks and A. Szabo, *Mol. Phys.*, 1988, **65**, 1409-1419.
68. T. Darden, D. York and L. Pedersen, *J. Chem. Phys.*, 1993, **98**, 10089-10092.
69. J.-P. Ryckaert, G. Ciccotti and H. J. Berendsen, *J. Comput. Phys.*, 1977, **23**, 327-341.
70. D. A. Pearlman, D. A. Case, J. W. Caldwell, W. S. Ross, T. E. Cheatham, S. DeBolt, D. Ferguson, G. Seibel and P. Kollman, *Comput. Phys. Commun.*, 1995, **91**, 1-41.
71. D. Bashford and D. A. Case, *Annu. Rev. Phys. Chem.*, 2000, **51**, 129-152.
72. M. F. Sanner, A. J. Olson and J. C. Spehner, *Biopolymers*, 1996, **38**, 305-320.
73. G. D. Hawkins, C. J. Cramer and D. G. Truhlar, *J. Phys.Chem*, 1996, **100**, 19824-19839.
74. A. Onufriev, D. Bashford and D. A. Case, *Proteins: Structure, Function, and Bioinformatics*, 2004, **55**, 383-394.
75. J. Mongan, C. Simmerling, J. A. McCammon, D. A. Case and A. Onufriev, *J. Chem. Theory. Comput*, 2007, **3**, 156-169.
76. H. Nguyen, D. R. Roe and C. Simmerling, *J. Chem. Theory. Comput*, 2013, **9**, 2020-2034.
77. T. Hou, J. Wang, Y. Li and W. Wang, *J. Chem. Inf. Modell*, 2011, **51**, 69-82.

78. T. Hou, J. Wang, Y. Li and W. Wang, *J. Comput. Chem*, 2011, **32**, 866-877.
79. J. J. Stewart, *J. Mol. Modell*, 2007, **13**, 1173-1213.

View Article Online
DOI: 10.1039/C9CP03598B